LETTERS
PUBLISHED ONLINE: 29 MAY 2011 | DOI: 10.1038/NMAT3030
nature materials

Dirac cones induced by accidental degeneracy in photonic crystals and zero-refractive-index materials

Xueqin Huang[1†], Yun Lai[1,2†], Zhi Hong Hang[1†], Huihuo Zheng[1] and C. T. Chan[1*]

A zero-refractive-index metamaterial is one in which waves do not experience any spatial phase change, and such a peculiar material has many interesting wave-manipulating properties[1–10]. These materials can in principle be realized using man-made composites comprising metallic resonators[7] or chiral inclusions[11,12], but metallic components have losses that compromise functionality at high frequencies. It would be highly desirable if we could achieve a zero refractive index using dielectrics alone. Here, we show that by employing accidental degeneracy, dielectric photonic crystals can be designed and fabricated that exhibit Dirac cone dispersion at the centre of the Brillouin zone at a finite frequency. In addition to many interesting properties intrinsic to a Dirac cone dispersion[13–19], we can use effective medium theory to relate the photonic crystal to a material with effectively zero permittivity and permeability. We then numerically and experimentally demonstrate in the microwave regime that such dielectric photonic crystals with reasonable dielectric constants manipulate waves as if they had near-zero refractive indices at and near the Dirac point frequency.

Electronic[13–15] and photonic systems[16–23] with Dirac cones in the band structure possess remarkable wave transport properties[13–19]. Materials with a zero refractive index also possess very interesting wave manipulation characteristics[1–10]. These two seemingly unrelated classes of material are actually related in a subtle way. For a dispersive homogeneous material in which the frequency-dependent permittivity (ε) and permeability (μ) are simultaneously zero at a particular frequency ω_0, it can be shown that the dispersion is linear and cone-like at $\mathbf{k}=0$ at ω_0 (ref. 16). As $\varepsilon(\omega)=\mu(\omega)=0$ implies an effectively zero refractive index, there is an intimate relationship between zero refractive index and Dirac cone dispersion. However, a Dirac cone dispersion does not necessarily imply a zero refractive index. Although it is well known that some photonic crystals (PCs) have Dirac cone dispersion[17–23], the Dirac points are at the zone boundary, and these cannot be mapped to a zero-refractive-index system. A Dirac cone at $\mathbf{k}=0$ is required, which is difficult to realize because the dispersions are generally quadratic at the centre of the Brillouin zone, making a linear dispersion at $\mathbf{k}=0$ (a necessary condition for a Dirac cone) the exception rather than the rule. In addition, even if we can design a PC with a Dirac cone at $\mathbf{k}=0$, it can be mapped to an $\varepsilon_{\text{eff}}=\mu_{\text{eff}}=0$ system only if an effective medium theory[24] can be satisfactorily applied.

The purpose of this work is to establish the conditions for realizing Dirac cones at $\mathbf{k}=0$ in dielectric PCs. We propose to show by numerical simulations and through microwave experiments that

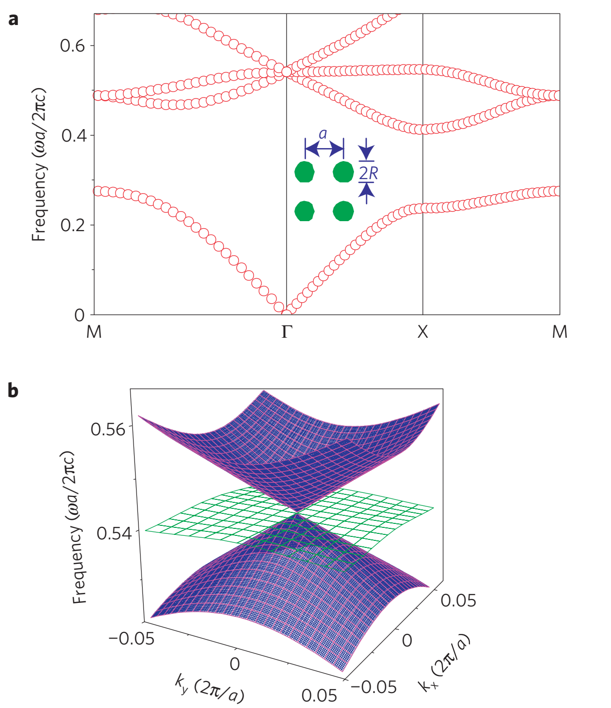

Figure 1 | The band structure of a two-dimensional photonic crystal with a square lattice. a, The band structure for a 2D PC constructed of cylinders with radius $R=0.2a$, relative permittivity $\varepsilon=12.5$ and permeability $\mu=1$. Two linear dispersion bands intersect at the Dirac point $f=0.541c/a$, with an additional flat band. **b**, Three-dimensional dispersion surfaces near the Dirac point frequency of the band structure shown in **a**, showing the relationship between the frequency and wave vectors (k_x and k_y). The linear bands (purple) form cones that touch at the Dirac point. There is an additional sheet (green) of quasi-longitudinal modes.

an effective medium theory can indeed link such 'Dirac cone at $\mathbf{k}=0$' PCs with reasonable dielectric constants to a $\varepsilon_{\text{eff}}=\mu_{\text{eff}}=0$ system, and that purely dielectric PCs can behave as if they had a zero refractive index.

Figure 1a shows that linear dispersion and Dirac cones can be obtained at the Γ point ($\mathbf{k}=0$) using a simple two-dimensional (2D) PC consisting of a square lattice of dielectric rods. The band structures are calculated for the transverse magnetic (TM) polarization with the electric field along the rod axis. Here, the

[1]Department of Physics, Hong Kong University of Science and Technology, Clear Water Bay, Kowloon, Hong Kong, China, [2]Department of Physics, Soochow University, 1 Shizi Street, Suzhou 215006, China. [†]These authors contributed equally to this work. *e-mail: phchan@ust.hk.

© 2011 Macmillan Publishers Limited. All rights reserved

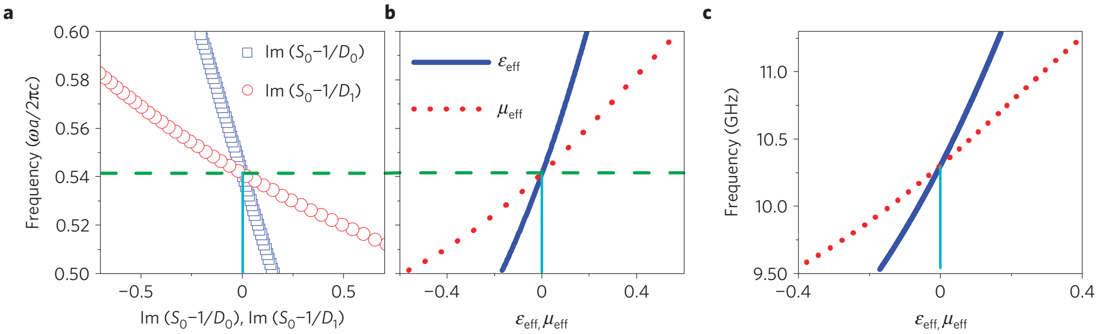

Figure 2 | Accidental degeneracy conditions and effective parameters from effective medium theory. a, The value of the imaginary part of the scattering coefficients $S_0 - 1/D_0$ (blue open squares) and $S_0 - 1/D_1$ (red open circles) as a function of frequency for the PC with the band structure shown in Fig. 1. Note that the condition $S_0 = 1/D_0 = 1/D_{\pm 1}$ is satisfied at the Dirac point. **b**, The effective permittivity ε_{eff} (blue solid line) and permeability μ_{eff} (red dotted line) as a function of frequency for the 2D PCs obtained using effective medium theory. Here, the cylinders have $R = 0.2a, \varepsilon = 12.5, \mu = 1$, as in Fig. 1. Note that $\varepsilon_{eff} = \mu_{eff} = 0$ at the Dirac point frequency (marked by the green dashed line). **c**, The effective permittivity ε_{eff} (blue solid line) and permeability μ_{eff} (red dotted line) as function of frequency (GHz) for a PC with $a = 17$ mm, $R = 3.75$ mm, $\varepsilon = 8.8$ and $\mu = 1$. Note that $\varepsilon_{eff} = \mu_{eff} = 0$ at the Dirac point frequency of this PC as well.

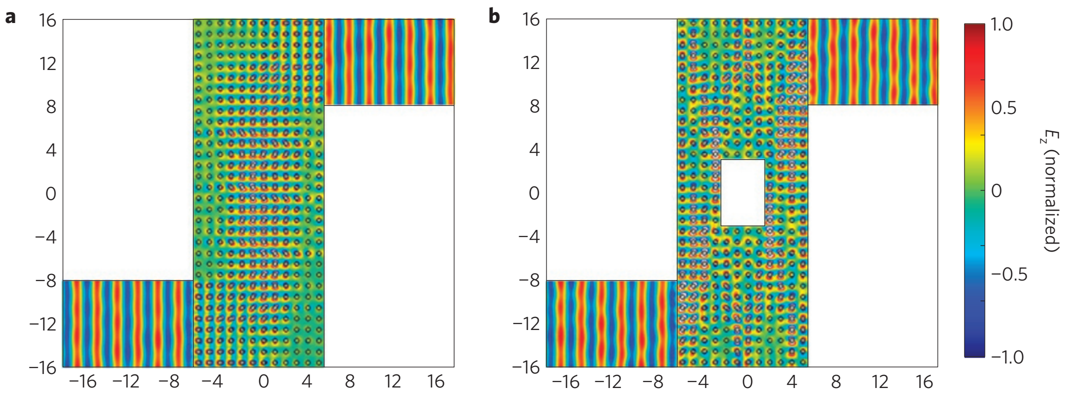

Figure 3 | Simulations demonstrating that waves can turn through a bent waveguide with and without embedded obstacles. a, The numerically simulated field distribution for waves incident at the lower left, turning through a 90° bend in a channel filled with 2D PCs, and exiting from the upper right channel. **b**, A PMC object marked by solid black lines is inserted inside the 2D PC array. The incident wave has a plane wavefront, and the boundary walls are PMCs. The incident frequency is equal to the Dirac point frequency $0.541c/a$. Note that in both cases the wave turns through the bends with little distortion.

lattice constant and the speed of light are denoted by a and c, and the radius and relative permittivity of the cylinders are set at $R = 0.2a$ and $\varepsilon = 12.5$, respectively. Two branches with linear dispersion intersect at a triply-degenerate point at $\mathbf{k} = 0$ (with frequency $f = 0.541c/a$), forming a Dirac cone. There is an additional flat branch intersecting the Dirac point. That flat band corresponds to a dipolar mode with its magnetic field polarized parallel to the wave vector $\mathbf{k}$ near $\mathbf{k} = 0$ (see the Supplementary Information). Thus it is a magnetic longitudinal mode near the Γ point. The Dirac cone modes comprise a dipolar mode with its magnetic field polarized perpendicular to $\mathbf{k}$ and a monopolar mode. A Dirac cone at the Γ point can also be found in a PC with a triangular lattice, as shown in the Supplementary Information. To illustrate such Dirac cones visually, the dispersion surfaces for the square lattice are plotted in Fig. 1b and for the triangular lattice in the Supplementary Information. There are clearly Dirac cones at the Γ point (purple) and a flat sheet (green) crossing the Dirac point.

The Dirac cones at the K point in electronic graphene[13–15] and in PCs (refs 17–23) with a triangular lattice that have been studied previously are consequences of the lattice symmetry. However, lattice symmetry alone gives only zero group velocity and hence quadratic dispersion at $\mathbf{k} = 0$. A Dirac cone at $\mathbf{k} = 0$ requires linear dispersion, which can be induced by accidental degeneracy. The condition for the existence of an 'accidental-degeneracy-induced Dirac point' (ADIDP) can be established using multiple scattering theory (MST). For the system under consideration, it is sufficient (see Supplementary Information) to consider dipolar ($m = \pm 1$) and monopolar ($m = 0$) terms, where m is the angular momentum number. The MST equations can be written in matrix form as:

$$\begin{pmatrix} S_0 - 1/D_{-1} & -S_1 & S_2 \\ -S_{-1} & S_0 - 1/D_0 & -S_1 \\ S_{-2} & -S_{-1} & S_0 - 1/D_1 \end{pmatrix} \cdot \begin{pmatrix} b_{-1} \\ b_0 \\ b_1 \end{pmatrix} = 0 \qquad (1)$$

where D_m and b_m are the T-matrix and Mie scattering coefficients respectively and S_m denotes the lattice sum with $S_{-m} = -S_m^*$. The cylindrical symmetry of the cylinders ensures that $D_1 = D_{-1}$, and lattice symmetry requires that $S_{\pm 1} = S_{\pm 2} = 0$ at $\mathbf{k} = 0$ for the square lattice. Solving equation (1) yields a monopolar eigenstate at frequency ω_m, where $S_0 - 1/D_0 = 0$, and doubly-degenerate dipolar eigenstates at a different frequency ω_d, where $S_0 - 1/D_{\pm 1} = 0$.

The dispersion near $\mathbf{k} = 0$ can be obtained by using perturbation methods (Supplementary Information). In general, $D_0 \neq D_{\pm 1}$ and the dispersion will have three branches, one branch corresponding to monopolar modes and two dipolar branches, all the branches with quadratic dispersion. If, however, there is accidental degeneracy such that $\omega_m = \omega_d = \omega^*$, or equivalently $S_0 = 1/D_0 = 1/D_{\pm 1}$, the dispersion near $\mathbf{k} = 0$ changes such that one solution has dispersion $\omega_1 - \omega^* = 0 + O(\delta k^2)$, corresponding

© 2011 Macmillan Publishers Limited. All rights reserved

to a band of quadratic dispersion that is almost flat near the Γ point, and two solutions that have a leading linear term of the form $\omega_{2,3} - \omega^* = \pm v_g \delta k + O(\delta k^2)$, corresponding to linear bands with opposite and non-zero group velocities $\pm v_g$. This, therefore, establishes theoretically that Dirac-like linear dispersion can be induced by accidental degeneracy. For a given value of permittivity and a given lattice constant, the condition $S_0 = 1/D_0 = 1/D_{\pm 1}$ can be achieved at a specific rod radius, and the resulting degeneracy is 'accidental', as is not a consequence of symmetry.

Figure 2a shows the calculated values of the imaginary part of $S_0 - 1/D_0$ and $S_0 - 1/D_1$ (here $S_0 - 1/D_0$ and $S_0 - 1/D_1$ are purely imaginary numbers, see Supplementary Information) as a function of frequency for the parameters shown in Fig. 1a. Clearly the condition $S_0 = 1/D_0 = 1/D_{\pm 1}$ is indeed satisfied at the Dirac point frequency $f = 0.541c/a$, and hence $S_0 = 1/D_0 = 1/D_{\pm 1}$ is the 'design condition' to obtain a Dirac cone at $\mathbf{k} = 0$ for PCs composed of cylindrical rods.

Is it possible, then, to describe the physics of the Dirac cone with an effective medium theory, and if so, what would it be? Note that an effective medium description would obviously be difficult for Dirac cones at the zone boundaries[17–23], but as the Dirac cones in this system are located at $\mathbf{k} = 0$, an effective medium description should be possible if the Dirac point is at a low enough frequency, which can always be achieved by using a material with a high enough dielectric constant. The question is how far this can be pushed using reasonable values of ε. To answer that question, we applied effective medium theory[24] to calculate the effective medium parameters for the structure shown in Fig. 1 with dielectric cylinders with $\varepsilon = 12.5$. The effective permittivity ($\varepsilon_{\mathrm{eff}}$) and permeability ($\mu_{\mathrm{eff}}$) as a function of frequency are shown in Fig. 2b, and $\varepsilon_{\mathrm{eff}}$ and μ_{eff} indeed intersect at zero at the Dirac point. In addition, Fig. 2a shows that the frequency at which $\varepsilon_{\mathrm{eff}} = \mu_{\mathrm{eff}} = 0 (\omega a/2\pi c = 0.541)$ is precisely the accidental degeneracy frequency defined by $S_0 = 1/D_0 = 1/D_{\pm 1}$. So, if the effective medium theory is a good description, a PC with a Dirac cone at the Γ point is an effective zero-refractive-index material with $\varepsilon_{\mathrm{eff}} = \mu_{\mathrm{eff}} = 0$ at the Dirac point. Since $\varepsilon_{\mathrm{eff}}$ and μ_{eff} approach zero simultaneously and linearly, the effective impedance of such a PC is a finite constant and the group velocity is also non-zero there. In addition, the PC system involves dielectrics alone and therefore will be low loss, which is an advantage at optical frequencies. We note that nano-scale dielectric (for example Si) pillar arrays can be fabricated[25].

PCs have some interesting wave manipulation properties at frequencies near the Dirac point. When a homogeneous zero-index material fills a waveguide, waves can tunnel through channels with unusual shapes[1]. Can a PC with the band structure shown in Fig. 1 support the same behaviour? Figure 3a shows numerical simulations which demonstrate that at the Dirac point frequency, waves incident from the lower left channel can turn round a 90° bend and emerge through the upper right exit channel with little distortion. The channels have boundary walls that are perfect magnetic conductors (PMCs). It is also known that an embedded object with PMC boundaries is invisible inside an $n = 0$ channel[9]. Figure 3b shows that if an object with PMC boundary conditions is inserted into the channel, the wave passes through the channel as if the obstacle were not there, manifesting the cloaking effect.

Figure 4 illustrates an experimental demonstration of the waveguiding properties of the PC. The square lattice PC was made of alumina rods 3.75 mm in radius and the lattice constant was 17 mm. Instead of $\varepsilon = 12.5$, as in Figs 1 and 3, alumina rods with $\varepsilon = 8.8$ were chosen, as these were readily available to us. The corresponding Dirac point frequency is 10.3 GHz. According to the effective medium formulae[24], the corresponding effective permittivity and permeability should still be simultaneously zero at the Dirac point (Fig. 2c). A cutaway view of the experimental set-up is shown in Fig. 4a (see Methods). Figure 4b shows the measured field distribution with microwaves incident from the left impinging on the PC (dielectric rods marked in yellow) with the central region replaced by a fairly large 40 mm × 40 mm metal obstacle (blue coloured square). As the walls were lined with a high-impedance surface[26] (see Methods), the incident wave had a plane wavefront.

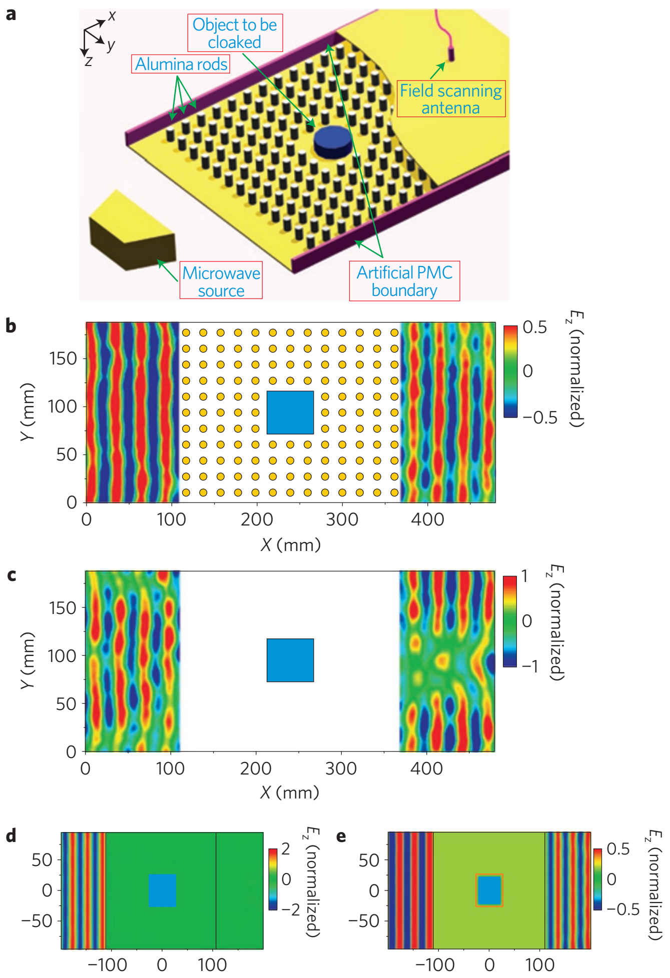

Figure 4 | Microwave experiment to illustrate the cloaking effect. a, A cutaway view of the experimental set-up exposing the PC formed of alumina rods used to realize cloaking inside a channel with the Dirac point at $f = 10.3$ GHz. **b**, The E_z field distribution observed at 10.3 GHz outside a PC (each rod in yellow) containing a 40 × 40 mm metallic obstacle (blue), normalized to the incident plane wave. **c**, A control experiment with all rods removed. **d**, Simulation results for a homogeneous $\varepsilon = \mu = 0$ medium (in green) in direct contact with an embedded metallic block (blue), which has the same size as that used in the experiment. Note the almost perfect reflection. **e**, Almost perfect transmission can be achieved by adding a thin layer of air between the boundary (orange) and the metallic block (blue). This simulation result corresponds to the experimental observation in **b**.

The measured fields on the right-hand side of the PC show that the microwaves simply passed through the PC, preserving their plane wave character as if the metal block were not there. Figure 4c shows that if the PC surrounding the metal block is removed, the metal obstacle will cast a clear shadow on the exit side and the plane wavefront is destroyed. Comparing Fig. 4b and c shows that such a PC at the Dirac point frequency can guide waves around an obstacle inside a channel. This also corroborates the recent result[27,28] that transmission through a zero-index metamaterial can be tuned by the details of the embedded defect.

Figure 4d and e show numerical simulations of a wave impinging on a homogenous $\varepsilon = \mu = 0$ medium (green coloured region) with

© 2011 Macmillan Publishers Limited. All rights reserved

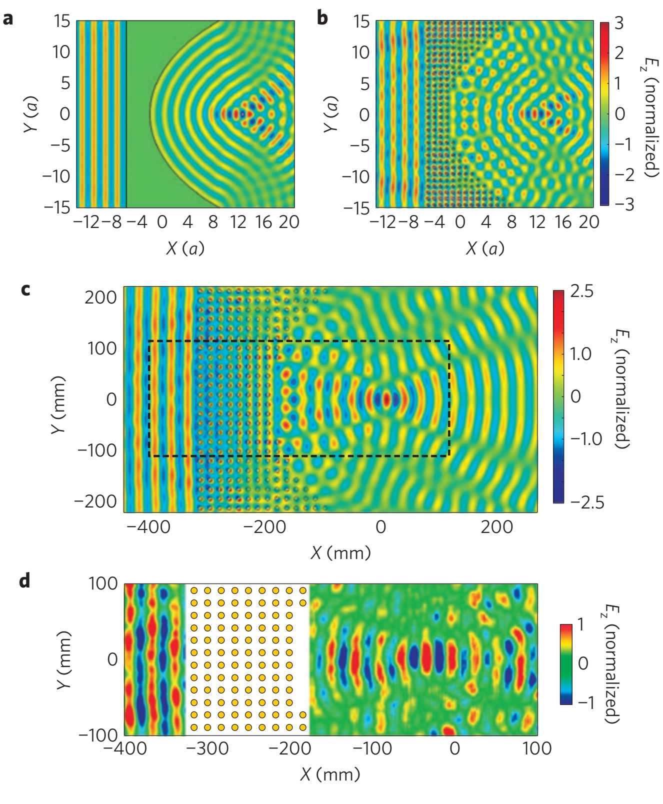

Figure 5 | Simulations and microwave experiment demonstrating waves passing through the PC with almost zero phase change. a,**b**, The numerically simulated field distribution for a homogeneous $\varepsilon = \mu = 0$ medium (**a**) and a 2D PC (**b**) as a lens. The incident wave has a plane wavefront coming from the left. The incident frequency is at the Dirac point with $f = 0.541c/a$. **c**,**d**, The simulation (**c**) and experimental measurements (**d**) of the field distribution for the alumina rod PC at 10.1 GHz. Owing to the limitations of the translation stage, only the centre part of field was scanned (corresponding to the dashed region in **c**).

an embedded metal block (blue coloured square). Figure 4d shows that if the embedded metal is in direct contact with the $\varepsilon = \mu = 0$ medium there is perfect reflection[9]. In Fig. 4e, the simulation result shows that there is almost perfect transmission if there is a thin layer of air (the region between the orange boundary and the blue square) separating the metal block and the $\varepsilon = \mu = 0$ domain. The experimental results actually correspond to the situation shown in Fig. 4e. One signature property of a zero-index material is that a wave can pass through it with no change in phase. This peculiar property is illustrated in the numerical simulation shown in Fig. 5a, which shows the focusing property of a concave lens made of a homogeneous $\varepsilon = \mu = 0$ medium. A plane wave is incident from the left, and as there is no phase change across the medium, the phase is the same on the concave surface, leading to the formation of a focal point to the right of the lens[2]. In Fig. 5b the homogeneous medium is replaced by a 2D PC with the configuration and band structure shown in Fig. 1. At the Dirac point frequency there is also a focal point to the right, and the field pattern is similar to the homogeneous case. Figure 5c shows numerical simulations near the Dirac point frequency for a PC with an ADIDP in which the dielectric cylinders are alumina with $\varepsilon = 8.8$. The focusing effect is still evident.

Microwave experiments were performed to demonstrate the focusing effect shown in Fig. 5c, the measured field patterns of which are shown in Fig. 5d. Note that both the simulations and the experiments employed absorbing boundaries and the sample size in the experiments was the same as in the simulation. Due to the size limitations of our translation stage, field patterns could be measured only in the region marked by the dashed lines in Fig. 5c. The reasonable agreement between the simulation results (Fig. 5c) and the experimental observations (Fig. 5d) provide evidence that zero phase change can indeed be achieved with a Dirac cone medium.

In summary, this study has established the conditions for obtaining a Dirac cone at $\mathbf{k} = 0$ in a dielectric PC. The results suggest that such PCs can be used to realize zero-refractive-index materials using non-metallic elements. The results also highlight yet another interesting implication of having a Dirac cone in the band structure.

Methods

Theory and simulation. The band structure results shown in Fig. 1a were calculated using the multiple scattering theory (MST), which has been used extensively in previous studies of two-dimensional photonic crystals (see for example ref. 29). The effective medium results were calculated using an MST-based effective medium theory, following the method detailed in ref. 24. The numerical simulation results shown in Figs 3, 4d,e and 5a–c were prepared using the numerical solver 'COMSOL Multiphysics'.

Fabrication of high-impedance surfaces. High-impedance surface boundary walls were employed in the experiment shown in Fig. 4. Such surfaces are widely used as a reflection ground plane for low-profile antennas[26]. By incorporating surface texture on the top surface, the reflection phase of the high-impedance surface can be tuned to be zero at the design frequency. As for this particular zero-reflection phase for an electric field parallel to the surface, the high-impedance surface served as an artificial perfect magnetic conductor (PMC) boundary at which the electric field parallel to the boundary reflects in-phase. The high-impedance surface was fabricated using double-sided photo-resist FR4 printed circuit board with a thickness of 1.6 mm and 35 μm of copper on both sides. One side was covered with an array of 3.1 mm × 3.1 mm copper patches with a periodicity of 4 mm, and the other side of the board was covered by a continuous copper layer. The zero-reflection frequency was designed to be at the Dirac point frequency of the alumina rod PC, 10.3 GHz. The bandwidth of operation was 1 GHz, defined as the frequency range where the reflection phase varied between −90° and 90°. The length of the high-impedance surface was 450 mm in the x direction (Fig. 4a) for the whole parallel-plate waveguide, and the height (along the z direction) was 16 mm.

Experimental set-up. A PC consisting of a 13 × 11 array of alumina rods (Fig. 4a) was assembled in the xy plane in a parallel-plate waveguide composed of two flat metallic (aluminium) plates separated by 16 mm. The PC array was fixed to the lower metal plate. Microwaves were introduced through a double-ridged microwave horn. The boundaries perpendicular to the wave propagation direction (x direction) were high-impedance surfaces, serving as artificial PMC boundaries. The whole experimental chamber can be considered as a waveguide that supports transverse electromagnetic modes.

As shown in Fig. 4b, in the centre of the PC, a 3 × 3 section of the alumina rods was replaced by a 40 mm × 40 mm metallic block. A field-scanning antenna was fixed in a hole in the upper metal plate, and the whole upper metal plate and the antenna were mounted on an orthogonal linear translation stage so that the relative position of the antenna with respect to the PC could be translated in the xy plane. By stepping the upper plate and antenna in 1 mm × 1 mm increments in the xy plane, the field amplitude and phase could be recorded outside the PC in both the incident and transmitted regions. This experimental set-up could not measure the field distribution inside the PC. For the control experiment shown in Fig. 4c, the set-up was identical except that all the alumina rods were removed. In Fig. 4b,c, the metal obstacle is indicated (to scale) by a blue square, and the dielectric cylinders are indicated by yellow circles. The air region inside the PC, which could not be measured, is in white.

For the experimental results shown in Fig. 5d, a PC composed of a 14 × 24 array of alumina rods was assembled inside a larger parallel-plate waveguide with the high-impedance surface replaced by absorbing material. Some rods were removed to create a concave surface at the exit end to demonstrate the 'zero phase change' property.

Received 2 February 2011; accepted 18 April 2011; published online 29 May 2011

References

1. Silveirinha, M. & Engheta, N. Tunneling of electromagnetic energy through subwavelength channels and bends using ε-near-zero materials. *Phys. Rev. Lett.* **97,** 157403 (2006).
2. Alu, A., Silveirinha, M. G., Salandrino, A. & Engheta, N. Epsilon-near-zero metamaterials and electromagnetic sources: Tailoring the radiation phase pattern. *Phys. Rev. B* **75,** 155410 (2007).

© 2011 Macmillan Publishers Limited. All rights reserved

3. Silveirinha, M. & Engheta, N. Design of matched zero-index metamaterials using nonmagnetic inclusions in epsilon-near-zero media. *Phys. Rev. B* **75,** 075119 (2007).
4. Silveirinha, M. G. & Engheta, N. Theory of supercoupling, squeezing wave energy, and field confinement in narrow channels and tight bends using ε near-zero metamaterials. *Phys. Rev. B* **76,** 245109 (2007).
5. Alu, A., Silveirinha, M. G. & Engheta, N. Transmission-line analysis of ε-near-zero-filled narrow channels. *Phys. Rev. E* **78,** 016604 (2008).
6. Edwards, B., Alu, A., Silveirinha, M. G. & Engheta, N. Reflectionless sharp bends and corners in waveguides using epsilon-near-zero effects. *J. Appl. Phys.* **105,** 044905 (2009).
7. Liu, R. *et al.* Experimental demonstration of electromagnetic tunnelling through an epsilon-near-zero metamaterial at microwave frequencies. *Phys. Rev. Lett.* **100,** 023903 (2008).
8. Edwards, B., Alu, A., Young, M. E., Silveirinha, M. & Engheta, N. Experimental verification of epsilon-near-zero metamaterial coupling and energy squeezing using a microwave waveguide. *Phys. Rev. Lett.* **100,** 033903 (2008).
9. Hao, J., Yan, W. & Qiu, M. Super-reflection and cloaking based on zero index metamaterial. *Appl. Phys. Lett.* **96,** 101109 (2010).
10. Ziolkowski, R. W. Propagation in and scattering from a matched metamaterial having a zero index of refraction. *Phys. Rev. E* **70,** 046608 (2004).
11. Tretyakov, S., Nefedov, I., Sihvola, A., Maslovski, S. & Simovski, C. Wave and energy in chiral nihility. *J. Electromagn. Waves Appl.* **17,** 695–706 (2003).
12. Pendry, J. B. A chiral route to negative refraction. *Science* **306,** 1353–1355 (2004).
13. Novoselov, K. S. *et al.* Two-dimensional gas of massless Dirac fermions in graphene. *Nature* **438,** 197–200 (2005).
14. Zhang, Y., Tan, Y. W., Stormer, H. L. & Kim, P. Experimental observation of the quantum Hall effect and Berry's phase in graphene. *Nature* **438,** 201–204 (2005).
15. Neto, A. H. C., Guinea, F., Peres, N. M. R., Novoselov, K. S. & Geim, A. K. The electronic properties of graphene. *Rev. Mod. Phys.* **81,** 109–162 (2009).
16. Wang, L. G., Wang, Z. G., Zhang, J. X. & Zhu, S. Y. Realization of Dirac point with double cones in optics. *Opt. Lett.* **34,** 1510–1512 (2009).
17. Sepkhanov, R. A., Bazaliy, Y. B. & Beenakker, C. W. J. Extremal transmission at the Dirac point of a photonic band structure. *Phys. Rev. A* **75,** 063813 (2007).
18. Zhang, X. Observing zitterbewegung for photons near the Dirac point of a two-dimensional photonic crystal. *Phys. Rev. Lett.* **100,** 113903 (2008).
19. Diem, M., Koschny, T. & Soukoulis, C. M. Transmission in the vicinity of the Dirac point in hexagonal photonic crystals. *Physica B* **405,** 2990–2995 (2010).
20. Plihal, M. & Maradudin, A. A. Photonic band structure of a two-dimensional system: The triangular lattice. *Phys. Rev. B* **44,** 8565–8571 (1991).
21. Haldane, F. D. M. & Raghu, S. Possible realization of directional optical waveguides in photonic crystals with broken time-reversal symmetry. *Phys. Rev. Lett.* **100,** 013904 (2008).
22. Raghu, S. & Haldane, F. D. M. Analogs of quantum-Hall-effect edge states in photonic crystals. *Phys. Rev. A* **78,** 033834 (2008).
23. Ochiai, T. & Onoda, M. Photonic analog of graphene model and its extension: Dirac cone, symmetry, and edge states. *Phys. Rev. B* **80,** 155103 (2009).
24. Wu, Y., Li, J., Zhang, Z. Q. & Chan, C. T. Effective medium theory for magnetodielectric composites: Beyond the long-wavelength limit. *Phys. Rev. B* **74,** 085111 (2006).
25. Gabrielli, L. H., Cardenas, J., Poitras, C. B. & Lipson, M. Silicon nanostructure cloak operating at optical frequencies. *Nature Photon.* **3,** 461–463 (2009).
26. Sievenpiper, D., Zhang, L., Broas, R. F. J., Alexopulos, N. G. & Yablonovitch, E. High-impedance electromagnetic surfaces with a forbidden frequency band. *IEEE Trans. Microw. Theory Tech.* **47,** 2059–2074 (1999).
27. Nguyen, V. C., Chen, L. & Halterman, K. Total transmission and total reflection by zero index metamaterials with defects. *Phys. Rev. Lett.* **105,** 233908 (2010).
28. Jin, Y. & He, S. Enhancing and suppressing radiation with some permeability-near-zero structures. *Opt. Exp.* **18,** 16587–16593 (2010).
29. Nicorovici, N. A., Mcphedran, R. C. & Botten, L. C. Photonic band gaps for arrays of perfectly conducting cylinders. *Phys. Rev. E* **52,** 1135–1145 (1995).

Acknowledgements

This work is supported by Hong Kong RGC grant 600209. We thank W. J. Wen for providing microwave equipment.

Author contributions

X.H. and Y.L. did the calculations, Z.H.H. designed and performed all the experimental measurements, H.Z. helped with the calculations, and C.T.C. conceived the idea and wrote the manuscript.

Additional information

The authors declare no competing financial interests. Supplementary information accompanies this paper on www.nature.com/naturematerials. Reprints and permissions information is available online at http://www.nature.com/reprints. Correspondence and requests for materials should be addressed to C.T.C.

© 2011 Macmillan Publishers Limited. All rights reserved